Editors' Suggestion

Flow of quantum correlations in noisy two-mode squeezed microwave states

M. Renger,[1,2,*] S. Pogorzalek,[1,2] F. Fesquet,[1,2] K. Honasoge,[1,2] F. Kronowetter,[1,2,3] Q. Chen,[1,2] Y. Nojiri,[1,2] K. Inomata,[4,5] Y. Nakamura,[4,6] A. Marx,[1] F. Deppe,[1,2,7] R. Gross,[1,2,7,†] and K. G. Fedorov[1,2,‡]

[1]*Walther-Meißner-Institut, Bayerische Akademie der Wissenschaften, 85748 Garching, Germany*
[2]*Physik-Department, Technische Universität München, 85748 Garching, Germany*
[3]*Rohde & Schwarz GmbH & Co. KG, Mühldorfstraße 15, 81671 Munich, Germany*
[4]*RIKEN Center for Quantum Computing (RQC), Wako, Saitama 351-0198, Japan*
[5]*National Institute of Advanced Industrial Science and Technology, 1-1-1 Umezono, Tsukuba, Ibaraki 305-8563, Japan*
[6]*Department of Applied Physics, Graduate School of Engineering, The University of Tokyo, Bunkyo-ku, Tokyo 113-8656, Japan*
[7]*Munich Center for Quantum Science and Technology (MCQST), Schellingstr. 4, 80799 Munich, Germany*

(Received 27 July 2022; accepted 6 October 2022; published 15 November 2022)

We study nonclassical correlations in propagating two-mode squeezed microwave states in the presence of noise. We focus on two different types of correlations, namely, quantum entanglement and quantum discord. Quantum discord has various intriguing fundamental properties which require experimental verification, such as the asymptotic robustness to environmental noise. Here, we experimentally investigate quantum discord in propagating two-mode squeezed microwave states generated via superconducting Josephson parametric amplifiers. By exploiting an asymmetric noise injection into these entangled states, we demonstrate the robustness of quantum discord against thermal noise while verifying the sudden death of entanglement. Furthermore, we investigate the difference between quantum discord and entanglement of formation, which can be directly related to the flow of locally inaccessible information between the environment and the bipartite subsystem. We observe a crossover behavior between quantum discord and entanglement for low noise photon numbers, which is a result of the tripartite nature of noise injection. We demonstrate that the difference between entanglement and quantum discord can be related to the security of certain quantum key distribution protocols.

DOI: 10.1103/PhysRevA.106.052415

I. INTRODUCTION

Quantum communication and quantum computing protocols often employ entanglement as a nonclassical resource to provide improvement of information transfer and achieve a quantum speed-up in processing [1]. In this regard, entanglement plays a key role in realizing quantum error correction [2] and efficient quantum simulation [3], as well as in achieving quantum supremacy [4]. Prominent examples of quantum communication protocols are quantum key distribution [5], dense coding [6], or quantum teleportation [7,8], where entanglement is exploited for an efficient and unconditionally secure state transfer. However, entanglement represents only one particular quantum resource and does not capture all nonclassical correlations. In particular, quantum discord (QD) provides a more general measure of nonclassical correlations including entanglement [9]. Quantum discord may serve as a resource in multiple quantum information processing protocols such as deterministic quantum computing with one qubit (DQC1) [10,11], quantum sensing [12], and quantum illumination [13]. Furthermore, theoretical investigations imply that QD has multiple intriguing physical properties which still lack experimental verification, such as the asymptotic robustness against environmental noise and its relation to entanglement in mixed tripartite systems [14]. These two properties are the key focus of our experimental study. In particular, our experiments reveal that the process of noise injection into a bipartite quantum system necessarily creates multipartite quantum correlations with the environment. As a result, the noise suppresses quantum correlations in the bipartite system and simultaneously increases the correlations between one of the subsystems and the environment. We measure this effect by extracting a flow of locally inaccessible information (LII) [15]. This LII flow behaves fundamentally different as a function of noise for different subsystems. The more detailed investigation of the LII flow may be relevant for testing ideas related to quantum Darwinism [16,17], where correlations with different fragments of the environment eventually lead to an objective reality [18]. In addition, we demonstrate that LII is related to the unconditional security of the Gaussian quantum key distribution (QKD) protocol, described in Ref. [19].

The potential robustness of QD versus noise is extremely useful for various quantum communication protocols. In particular, unavoidable external fluctuations cause loss of quantum correlations, and thereby lower the efficiency of these protocols. Protocols based on quantum entanglement are particularly vulnerable to noise, since entanglement cannot survive significant noise levels, leading to the so-called sudden death of entanglement [20]. This is especially

*michael.renger@wmi.badw.de
†rudolf.gross@wmi.badw.de
‡kirill.fedorov@wmi.badw.de

important for quantum communication protocols in the microwave regime, as room temperature is associated with thousands of thermal noise photons with characteristic frequencies of several GHz [21]. Here, the expected asymptotic robustness of QD [22] against noise offers a natural path for quantum communication and sensing. An actual challenge is to find protocols capable of exploiting QD as a quantum resource. As such, the remote state preparation (RSP) protocol stands out as one of the prominent examples. RSP aims at the generation of a desired and known quantum state at a remote location with the assistance of classical communication and complementary nonclassical correlations [23]. A particular quantum advantage provided by RSP is associated with the smaller amount of classical information required to prepare a quantum state, as compared to a fully classical communication protocol. Another benefit of the quantum RSP scheme is the unconditional security of the feedforward signal [24]. In some scenarios, the RSP protocol appears to exploit QD as its nonclassical resource [9,25]. Finally, there is a class of quantum sensing protocols known as quantum illumination, where entangled light is used to detect the presence of a low-reflectivity object in a bright noisy background. Naturally, entanglement vanishes in this scenario, yet residual nonclassical correlations, captured by QD, persist. The latter seems to be connected to the quantum advantage of these quantum sensing schemes [13,26].

II. EXPERIMENT

In this paper, we experimentally study the effect of noise injection into one mode of a propagating two-mode squeezed (TMS) state which is distributed along two paths, A and B. A schematic illustration of this scenario is shown in Fig. 1(a). The TMS state is generated by superimposing two orthogonally squeezed microwave states at a symmetric microwave beam splitter. Then, we inject an uncorrelated broadband noise into path B. Finally, we perform a joint quantum state tomography, which allows us to extract full information about the two-mode quantum state [27,28]. We use the entanglement of formation (EOF), $\mathcal{E}_F$, as a measure for bipartite entanglement between parties A and B. We choose this specific entanglement measure since it exactly coincides with QD for pure states [29]. Simultaneously, EOF is directly related to QD via various monogamy relations, which eventually enables the connection of both quantities to LII [15,30]. For continuous-variable quantum systems, EOF quantifies the minimal amount of two-mode squeezing needed to prepare an entangled state, starting from a classical one by using local operations and classical communication [31]. In addition, we extract an asymmetric bipartite QD, D_A (D_B), between the two subsystems A and B. It is defined as the difference between their quantum mutual information I_{AB} and a one-way classical correlation $J_{A|B}$ ($J_{B|A}$),

$$D_A = I_{AB} - J_{A|B}, \quad D_B = I_{AB} - J_{B|A}, \tag{1}$$

and quantifies the nonlocal fraction of I_{AB} [32].

Figure 1(b) illustrates our experimental setup. We use two superconducting flux-driven Josephson parametric amplifiers (JPAs) operated at the frequency $\omega_0/2\pi = 5.323$ GHz for squeezed state generation. Each of the JPAs performs a

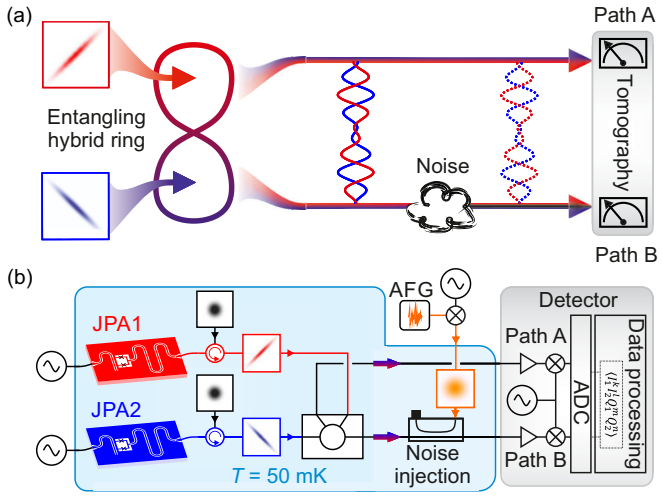

FIG. 1. (a) Scheme of two-mode squeezing and noise injection. Nonlocal correlations are generated by superposing two orthogonally squeezed states on a symmetric beam splitter to generate a path-entangled frequency-degenerate TMS state. The asymmetric noise injection couples the environment to one of the TMS subsystems. (b) Equivalent experimental setup consisting of two JPAs for squeezed state generation, a microwave hybrid ring, and a directional coupler for injection of white Gaussian noise generated at room temperature by an arbitrary function generator (AFG). The two-mode signal is detected with a heterodyne receiver setup and digitally processed to extract the statistical signal moments and reconstruct the corresponding covariance matrix.

squeezing operation on the incident weak thermal state [33]. By sending the respective squeezed states to a hybrid ring (symmetric microwave beam splitter), we generate a TMS microwave state. Here, entanglement is expressed in strong correlations between two nonlocal field quadratures [34–37]. Our final-state tomography is based on heterodyne measurements of paths A and B. After digital down-conversion and filtering, we extract the statistical field quadrature moments using a reference state reconstruction method [34,38]. Under the assumption that the reconstructed states are Gaussian, a local phase-space distribution is described by the resulting two-mode covariance matrix [34–36]. The photon number calibration of the experimental setup is obtained by using Planck spectroscopy [39]. In order to test the robustness of the nonclassical correlations against noise, we perform a controlled noise injection into one of the entangled paths [34–36]. The noise signal is generated using an arbitrary function generator (AFG), which produces a low-frequency white Gaussian noise with a specified bandwidth of 160 MHz. This noise signal is upconverted to the carrier frequency $\omega_0/2\pi$ and guided into the cryogenic setup. We implement the actual noise injection in one of the entangled paths with a directional coupler with coupling $\beta = -20$ dB. By varying the noise power emitted from the AFG, we probe both EOF and QD as a function of the injected noise photon number n for different JPA squeezing levels. The latter is defined as $S = -10\log_{10}(v_s/0.25)$, where v_s is the variance of the squeezed quadrature and the chosen vacuum reference is $v_{vac} = 0.25$. More details about the experimental setup are provided in Appendix A 1.

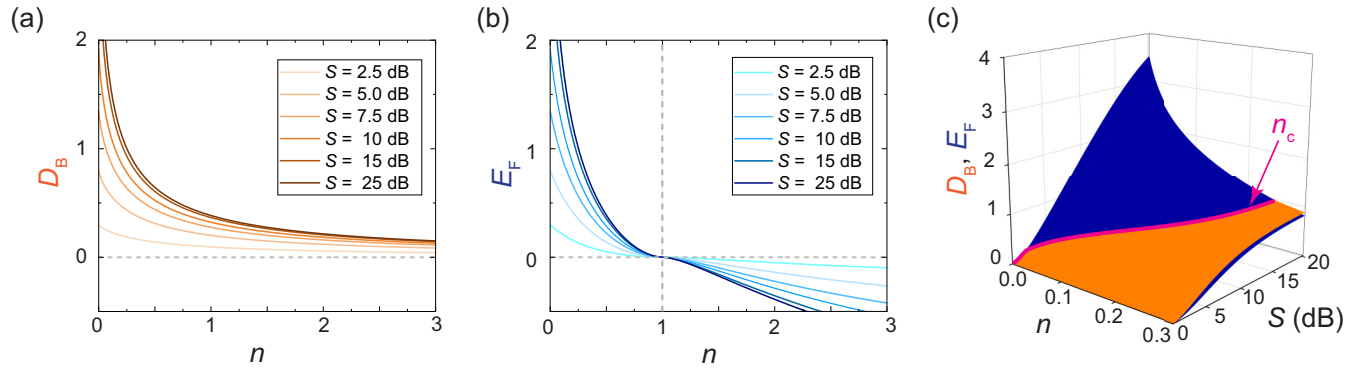

FIG. 2. Theoretical prediction of quantum correlations as a function of squeezing level S and noise photon number n. Panel (a) shows the quantum discord D_B, thereby demonstrating the asymptotic robustness, $D_B > 0$, for any finite level of noise and squeezing. Panel (b) shows the analytical lower bound E_F for EOF. At $n = 1$, as indicated by the vertical dashed line, we observe $E_F = 0$, independent of S, which demonstrates the sudden death of entanglement. In panel (c), E_F and D_B are plotted in the regime of $n \ll 1$, revealing a crossover region. Here, for low n, EOF is larger than QD. For increasing n, QD becomes larger than EOF. The crossover noise photon number n_c is depicted by the solid line, dividing the blue (dark gray) and orange (light gray) plane.

III. ENTANGLEMENT OF FORMATION AND QUANTUM DISCORD

Under the assumption that the state is Gaussian, EOF and QD can be extracted from the reconstructed two-mode covariance matrix V_{AB} [28,40]. In Ref. [27], it has been shown that a lower bound, E_F, for Gaussian EOF can be expressed as

$$E_F = s_\gamma[\cosh^2\gamma \ln(\cosh^2\gamma) - \sinh^2\gamma \ln(\sinh^2\gamma)] \leqslant \mathcal{E}_F, \tag{2}$$

where γ represents the minimally required amount of two-mode squeezing to disentangle the respective bipartite quantum state and $s_\gamma = \mathrm{sgn}(\gamma)$. For our analysis, we use an approximation $E_F \simeq \mathcal{E}_F$, which becomes exact in the case of symmetric local states A and B. The asymmetric Gaussian QD, D_A, corresponds to the correlation left after we perform a local measurement on subsystem B. It can be calculated as

$$D_A = f(\sqrt{I_2}) - f(\nu_+) - f(\nu_-) + f\left(\sqrt{E^{\min}_{A|B}}\right), \tag{3}$$

where I_2 denotes the second symplectic invariant of V_{AB} and $\nu_\pm$ are the corresponding symplectic eigenvalues [29]. The quantity $\sqrt{E^{\min}_{A|B}}$ describes the minimized conditional entropy and f is defined as $f(x) = (2x + \frac{1}{2})\ln(2x + \frac{1}{2}) - (2x - \frac{1}{2})\ln(2x - \frac{1}{2})$. A similar expression can be written for the quantum discord D_B, where the measurement is performed on system A. It can be shown that for pure quantum systems, i.e., in the limit of $n \to 0$, EOF and QD coincide [29]. Nevertheless, for mixed states, these quantities behave fundamentally different, as theory predicts asymptotic stability of QD, in contrast to EOF.

Figure 2 shows theoretically expected results for an idealized experiment with zero losses and noiseless JPAs. In Fig. 2(a) [Fig. 2(b)], we plot D_B (E_F) as a function of the average noise photon number n, injected to the TMS state, and the squeezing level S. We observe the expected asymptotic stability of QD, $D_B > 0$, and the sudden death of entanglement, $E_F < 0$, for $n > 1$. The latter effect can be understood by expressing γ in Eq. (2) analytically as

$$\gamma(r, n) = \frac{1}{2}\ln\left[\frac{e^{2r} + n}{1 + e^{2r}n}\right], \tag{4}$$

where r is the squeezing factor, which can be calculated by $r = S/(20\log_{10} e)$ for noiseless amplification by both JPAs. We observe that $\gamma(r, 1) = 0$, independent of r, indicating the sudden death of entanglement. In Fig. 2(c), we plot the theory values of E_F and D_B for low noise photon numbers and observe a crossover between EOF and QD. We denote the crossover point in terms of a corresponding noise photon number, n_c. This crossover point, $n_c > 0$, exists for any positive squeezing level S. This effect has been predicted in Refs. [41,42] and is a direct result of a tripartite nature of the noise injection. The latter implies that a correct quantum-mechanical description of noise necessarily requires one to take into account the environment E as a third interacting quantum system. For the tripartite system, it can be shown that EOF and QD are monogamous, i.e., that bipartite QD can only be increased by the simultaneous consumption of bipartite EOF and vice versa [30]. From this monogamic conservation relation, it has been shown that the difference between EOF and QD can be expressed as [15]

$$\Delta_A \equiv D_A - \mathcal{E}_F = \frac{1}{2}(\mathcal{L}_{B\to A\to E} - \mathcal{L}_{E\to A\to B}), \tag{5}$$

$$\Delta_B \equiv D_B - \mathcal{E}_F = \frac{1}{2}(\mathcal{L}_{A\to B\to E} - \mathcal{L}_{E\to B\to A}), \tag{6}$$

$$\Delta_{AB} \equiv \frac{D_A + D_B}{2} - \mathcal{E}_F = \frac{1}{2}\left(\mathcal{L}_{\binom{A}{B}\to E} - \mathcal{L}_{E\to\binom{A}{B}}\right), \tag{7}$$

where $\mathcal{L}_{X\to Y\to Z}$ denotes the flow of LII from the system X over Y to Z and $\mathcal{L}_{\binom{X}{Y}\to Z}$ ($\mathcal{L}_{Z\to\binom{X}{Y}}$) is the LII flow from (to) the bipartite system XY to (from) Z. As a result, if $\Delta_{AB} > 0$, more LII flows from the bipartite system AB to the environment E than vice versa.

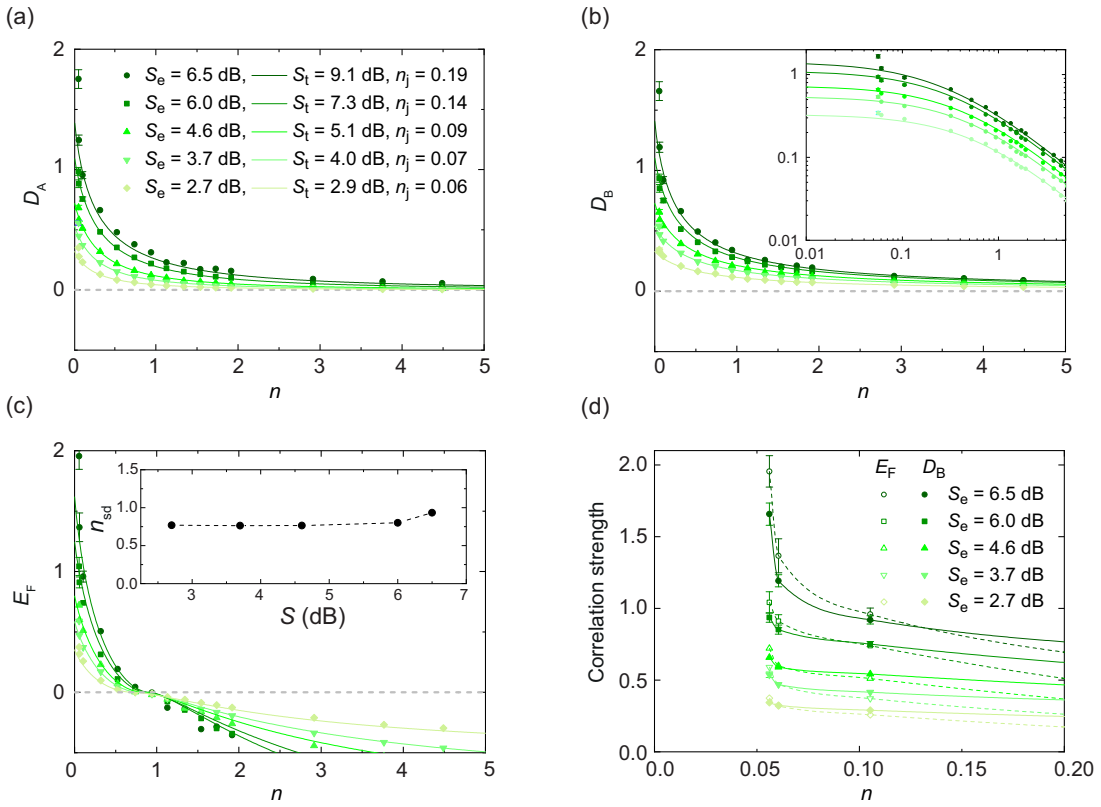

FIG. 3. (a) Experimentally obtained values of quantum discord D_A as a function of the injected noise photon number n for various squeezing levels S. Symbols indicate the measured data and lines are fits according to a realistic model, described in Appendix A 3, which takes a finite JPA noise into account. The quantity S_e denotes the experimentally determined squeezing level and S_t is the corresponding squeezing level, obtained by fitting the data by the theory prediction. The JPA noise n_j is extracted from the fit and is a function of gain. Although only shown for D_A, the fitted values for S_e and n_j are the same for D_B and E_F. (b) Experimentally obtained values of quantum discord D_B as a function of the injected noise photon number, n, for various squeezing levels. The inset shows the same data in a log-log plot. (c) Experimental EOF (symbols) and corresponding fits (lines) for various squeezing levels. We observe the sudden death of entanglement at $n_{sd} \simeq 1$. The inset shows that n_{sd} is independent of S, where n_{sd} is obtained from the experimental data using cubic Hermite spline interpolation. Error bars are obtained from the statistical measurement error and are only plotted if the error exceeds the symbol size. (d) Zoom in of experimental results for D_B and E_F for low noise photon numbers n and various squeezing levels S_e. Solid (dashed) lines are the result from a cubic Hermite spline interpolation between the measured values for D_B (EOF). Here, we observe the crossover behavior of QD and EOF, as predicted by the theory.

IV. RESULTS AND DISCUSSION

The experimentally determined QD values, D_A and D_B, are provided in Figs. 3(a) and 3(b) and the quantum entanglement measure E_F is shown in Fig. 3(c). The line plots correspond to a fit according to Eq. (3) for the QD and Eq. (2) for the EOF, where we take the finite JPA noise into account. The gain-dependent noise, added by the JPAs, is modeled by a power-law dependence, $n_j = \chi_1(G-1)^{\chi_2}$, where G represents the degenerate gain [43]. The coefficients χ_1 and χ_2 are treated as fit parameters. We find $\chi_1 = 0.05$ and $\chi_2 = 0.56$. In Fig. 3(a), we additionally show the experimentally determined squeezing level S_e, as well as the respective theoretical squeezing level S_t and fitted JPA noise n_j. We observe that the fits reliably reproduce the experimental data. More information about the fitting routine is given in Appendix A 3.

Furthermore, we find that the experimentally determined QD is always positive and converges towards zero for $n \to \infty$, thereby proving the asymptotic robustness against noise. In contrast to that, we find that E_F becomes zero already at a finite noise photon number $n_{sd} \simeq 1$, experimentally verifying the sudden death of entanglement. This value is an important fundamental noise threshold for two-mode squeezed light. The respective experimental values for n_{sd} as a function of squeezing are shown in the inset of Fig. 3(c). They have been extracted from the experimental data using cubic Hermite spline interpolation. We find that n_{sd} is independent of the squeezing level, as expected from theory. Note that the experimentally determined noise level for the sudden death of entanglement is lower than the theoretically predicted noise photon number of unity. This is a result from the finite noise added by the JPAs themselves. In addition to that, further deviations from ideal theory are caused by path losses and a pump crosstalk between the JPAs. However, these imperfections are not taken into account in the current fit model. The deviation of n_{sd} from constant behavior at $S = 6.5$ dB is a result from imperfect balancing of the TMS state due to pump leakage.

For most of the observed states, EOF appears to be smaller than QD. This can be understood by the fact that, by definition, QD describes more general nonlocal correlations than EOF. However, this simple relation is only true in the bipartite limit. When one considers the environment as a third party,

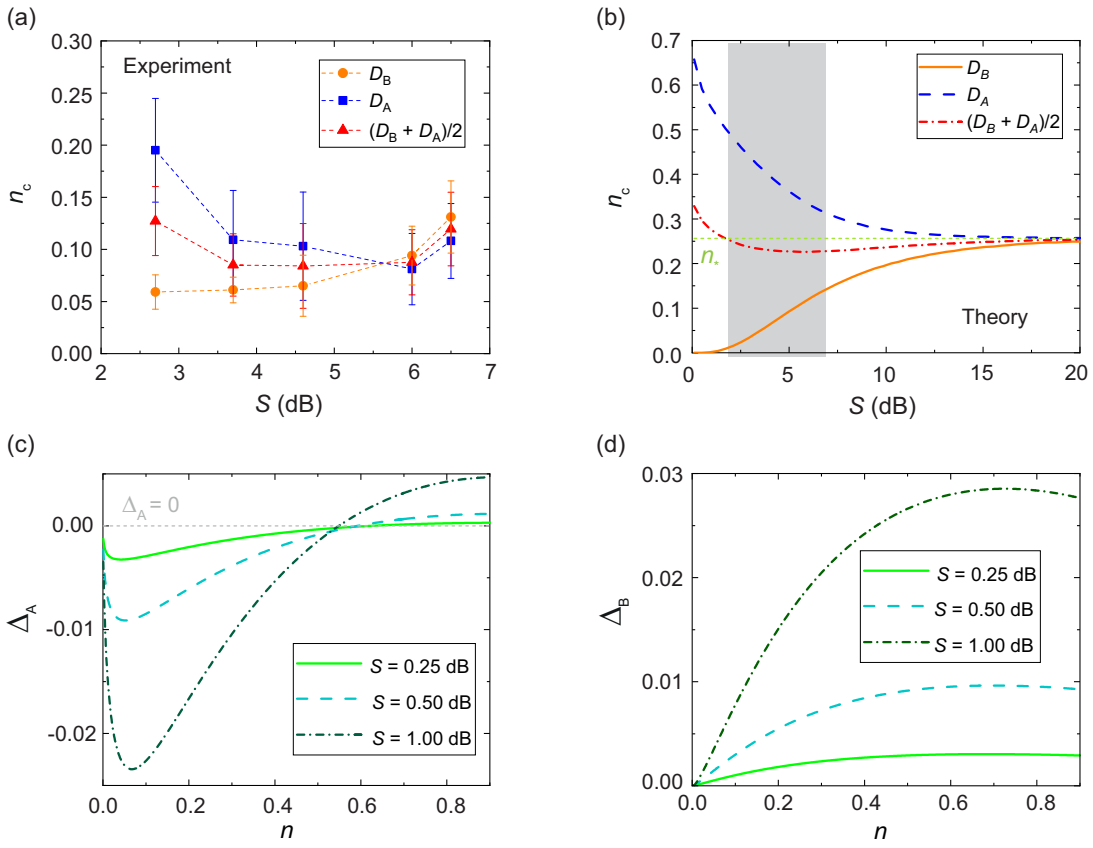

FIG. 4. (a) Experimentally determined crossover noise photon number, n_c, as a function of the squeezing level for D_A (blue squares) and D_B (orange dots). Red triangles represent the arithmetic mean of n_c for D_A and D_B, where we observe a minimum in the region of 5 dB. The error bars are determined from the experimental uncertainties of QD and EOF by randomized error sampling. (b) Theoretically predicted n_c for D_A (blue dashed line), D_B (orange solid line) for the case of an idealized (lossless and noiseless, $\beta \to 0$) experiment. In the case of D_A (D_B), n_c decreases (increases) monotonically with S. We observe a minimum for $S_{min} \simeq 5.73$ dB for the red dotted-dashed curve which corresponds to the arithmetic mean of both discords, D_A and D_B. In the limit $S \to \infty$, n_c converges to the same constant $n_* \simeq 0.26$ for D_A and D_B. The gray shaded region indicates the experimentally obtained squeezing levels, corresponding to panel (a). (c) Theoretical difference Δ_A between D_A and E_F as a function of the noise photon number n for various squeezing levels S. (d) Theoretical difference Δ_B between D_B and E_F as a function of the noise n for various squeezing levels S.

the relation between bipartite QD and EOF may change. In order to experimentally investigate the latter we investigate the regime of $n \ll 1$ in more detail. Here, theory predicts a crossover between EOF and QD, according to Fig. 2(c). To experimentally study this crossover region, we replot the measured D_B and E_F for noise photon numbers $n \leqslant 0.2$ in Fig. 3(d), revealing the intersection between EOF and QD, especially well observable for $S_e = 6.5$ dB. The solid (dashed) lines correspond to a cubic Hermite spline interpolation for D_B (E_F). From this interpolation, we determine the crossover noise photon number n_c as a function of squeezing. The same procedure is repeated for D_A and $D_{AB} \equiv (D_A + D_B)/2$. The corresponding results are plotted in Fig. 4(a) and the predictions based on an ideal (lossless and noiseless) model are depicted in Fig. 4(b). In the limit $S \to \infty$, we observe that $n_c \to n_* \simeq 0.26$ for D_A as well as for D_B. Furthermore, we find a qualitative agreement between experiment and theory for the dependence of n_c on the squeezing level S. Nevertheless, we observe that for D_A the experimentally determined values are lower than those predicted by theory. This deviation can be explained by the finite noise, losses, and crosstalk between the JPAs, since these effects are not taken into account in the ideal theory model. Furthermore, we note that we cannot experimentally investigate the whole range shown in Fig. 4(b), as larger squeezing levels are not experimentally achievable due to the gain-dependent noise added by the JPAs. As shown by the red dotted-dashed line in Fig. 4(b), the corresponding n_c for $(D_A + D_B)/2$ has a minimum at $n_{min} \simeq 0.23$, corresponding to $S_{min} = 5.7$ dB. Thus, when one attempts to maximize n_c in the bipartite system AB, it is not always beneficial to increase the squeezing level. Experimental data in Fig. 4(a) qualitatively reproduces this result.

Next, we investigate the asymmetric differences between EOF and QD, Δ_A, Δ_B, and Δ_{AB}, as a function of the noise photon number n. Figure 4(c) [Fig. 4(d)] shows the theoretically expected noise dependence of Δ_A (Δ_B) for various squeezing levels S. We observe that the quantities Δ_A and Δ_B behave fundamentally different in the limit of low noise. In particular, the crossover noise photon number n_c decreases monotonically with increasing S in the case of Δ_A, as can also be seen in Fig. 4(b). On the contrary, n_c shows a monotonic increase as a function of S for increasing Δ_B. This fundamental

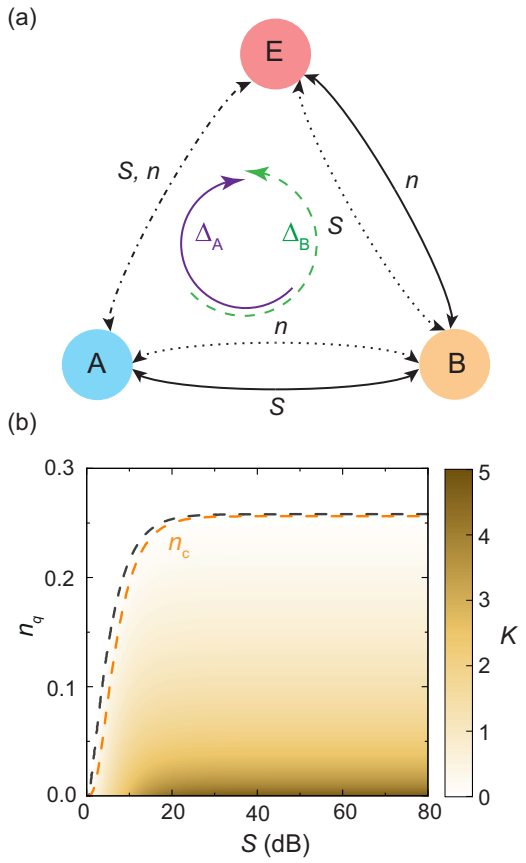

FIG. 5. (a) Schematic dependence of bipartite correlations between subsystems A, B, and E. Solid (dotted) black arrows indicate a monotonic increase (decrease) of bipartite correlations with a respective quantity. The dotted-dashed arrow, connecting A and E, indicates that correlations between these subsystems are not necessarily monotonic in S or n. The solid curved purple (dashed green) arrow indicates the LII flow B→A→E (A→B→E), described by Δ_A (Δ_B). (b) Theoretical secret key K as a function of the resource state squeezing level S and injected noise photon number n_q in the detected quadrature. Here, we assume a continuous-variable QKD protocol between A and B [19], where the environment acts as an eavesdropper. The black dashed line indicates the threshold separating the areas of positive secret keys (secure), $K > 0$, and negative keys (insecure), $K < 0$. The orange (light gray) dashed line shows the corresponding n_c for D_B as a function of S, which offers an intuitive explanation for the security of the QKD protocol on the language of the LII flow between the subsystems.

deviation can be understood by the fact that noise injection in B is a local process and directly leads to bipartite correlations between party B and environment E. In contrast, this local process only indirectly correlates A and E. Thus the bipartite correlations between B and E increase monotonically with n. Furthermore, the correlation between A and B monotonically decreases as a function of n. In contrast to that, correlations between A and E can only result from an interplay between squeezing S and noise n and are not necessarily required to be monotonic in these quantities. The scenario is schematically depicted in Fig. 5(a), where solid black arrows, connecting to systems X and Y with $X, Y \in \{A, B, E\}$, indicate a monotonic increase of correlations. The direction of the LII flow, described by Δ_A (Δ_B) according to Eq. (5) [Eq. (6)], is shown by the curved solid purple (dashed green) arrow. Note that Δ_A describes the net LII flow B → A → E and Δ_B describes the respective net flow A → B → E. Therefore, the fundamentally different behavior of these quantities as a function of n, as shown in Figs. 4(c) and 4(d), can be explained by the fact that in the case of Δ_B no direct bipartite correlations between A and E are required to establish an LII flow, in contrast to the case described by Δ_A.

Furthermore, the quantities Δ_A, Δ_B, and Δ_{AB} can become of practical interest for entanglement-based quantum key distribution (QKD) protocols [44], where an eavesdropper attempts to extract LII from a bipartite quantum system. In such a scenario, the subsystems A and B exploit quantum correlations to securely share a common secret key and the subsystem E can be related to an eavesdropper controlling the environment [45]. Then, the noise injection can be interpreted as the result of an entangling cloner attack performed by the eavesdropper [46]. It directly follows from Eq. (7) that the eavesdropper needs to add at least n_c noise photons to the system AB to get a positive net flow of LII. Numerically, we find that in the limit $S \to \infty$, we have $n_c \to n_* \simeq 0.26$ for Δ_A, Δ_B, and Δ_{AB}. In order to investigate this interrelation, we consider a Gaussian CV-QKD scheme described in Refs. [19,47] under the assumption of reverse reconciliation [48]. We consider a scenario where A and B share a TMS resource state and assume that the eavesdropper performs an entangling cloner attack via the directional coupler. The resulting secret key which quantifies the amount of exchanged secure information can be calculated as

$$K = I_s(\mathrm{A} : \mathrm{B}) - \chi_E, \tag{8}$$

where $I_s(\mathrm{A} : \mathrm{B})$ denotes the Shannon mutual information between A and B and χ_E represents the eavesdropper's Holevo quantity [48,49]. Figure 5(b) shows the theoretically expected K as a function of the resource state squeezing level S and noise photon number n_q in the detected quadrature for the case when B performs a homodyne detection on his part of the entangled state. Note that, in contrast to the full noise, n, we only consider noise n_q, added to the detected quadrature, q. This is because the homodyne detection is equivalent to phase-sensitive amplification and measurement of a certain quadrature which inherently deamplifies the other quadrature [29]. Consequently, only the noise in the amplified quadrature has an effect on the measurement result. We observe that, similar to the quantities Δ_A, Δ_B, and Δ_{AB}, the threshold value for n_q, when we obtain a positive secret key, converges towards $n_q \simeq 0.26$ for $S \to \infty$. We numerically find that this asymptotic value approximately coincides with n_*. Thus we can only obtain a positive secret key in the high squeezing limit if the noise, added to the detected quadrature, is lower than the threshold n_*, required for a positive LII flow to the eavesdropper. As a result, the difference between QD and EOF can act as an indicator whether it is possible to obtain a positive secret key or not. More details about the calculation of K are provided in Appendix A 2.

In summary, we have investigated the influence of local noise injection in propagating TMS microwave states on quantum discord correlations and quantum entanglement quantified via the entanglement of formation measure. We

have experimentally verified the sudden death of entanglement around theoretically predicted values of approximately one injected noise photon, independent of the squeezing level. Furthermore, we have experimentally demonstrated that in strong contrast to entanglement, QD is asymptotically robust against noise. In addition, we have measured the theoretically predicted crossover between EOF and QD for small noise photon numbers, which is a result of the tripartite nature of mixed TMS states. Since the difference between QD and EOF can be related to the net flow of LII, it may be used to assess the security of certain QKD protocols based on squeezed states. We have demonstrated that the locality of noise injection implies a fundamental difference between the LII flows A→B→E and B→A→E. Finally, the demonstrated results on the robustness of QD against noise are relevant for the DQC1 quantum computation approach and quantum illumination protocols. These applications can be viewed as a motivation to intensify the search for quantum information processing, communication, and sensing protocols exploiting QD as a quantum resource. Such protocols would be inherently resistant to noise in contrast to entanglement-based approaches which suffer from the sudden death of entanglement.

ACKNOWLEDGMENTS

We acknowledge support by the German Research Foundation via Germany's Excellence Strategy (EXC-2111-390814868), the Elite Network of Bavaria through the program ExQM, the EU Flagship project QMiCS (Grant No. 820505), and the German Federal Ministry of Education and Research via the project QUARATE (Grant No. 13N15380), the project QuaMToMe (Grant No. 16KISQ036), JSPS KAKENHI (Grant No. 22H04937), and JST ERATO (Grant No. JPMJER1601). This research is part of the Munich Quantum Valley, which is supported by the Bavarian state government with funds from the Hightech Agenda Bayern Plus.

APPENDIX

1. Experimental setup

The JPAs are thermally stabilized at 50 mK to guarantee steady squeezing and noise properties. We pump the JPAs using Rohde&Schwarz SGS100A microwave sources and pulse the pump signal using a data timing generator (DTG) [24,34,50,51]. Here, the TMS state is generated by superimposing two orthogonally squeezed states with equal squeezing levels using a cryogenic hybrid ring, acting as a 50:50 beam splitter. The resulting TMS state at the hybrid ring output then locally looks like thermal noise but shows strong nonlocal correlations in the covariances. The photon number in the TMS state is calibrated using the Planck spectroscopy [39], which is realized by sweeping the temperature of a heatable 30 dB attenuator in the temperature range of 40 mK–600 mK. By using this heatable attenuator as a self-calibrated cryogenic photon source, we can directly map the detected voltage in the output signal to the photon number in the cryogenic quantum signal [39]. One part of the TMS state is transmitted to a directional coupler (CPL-4000-8000-20-C, Miteq/Sirius) with coupling $\beta = -20$ dB. The coupled port of the directional coupler is used to inject white broadband noise into the system, which is generated using a Keysight 81160A arbitrary waveform generator (AFG). The generated noise has a bandwidth of 160 MHz and is upconverted to the signal reconstruction frequency of $\omega_0/2\pi = 5.323$ GHz using a local oscillator (LO). Due to the low signal level, the output signal needs to go through multiple amplification stages consisting of a cryogenic high-electron-mobility transistor (HEMT) amplifier and additional room-temperature amplifiers, which are stabilized in temperature by a Peltier cooler. The overall noise of the detection chain is determined by the HEMT, which results from its high gain (∼40 dB). Frequency-resolved measurements are performed using a vector network analyzer (VNA) and the reconstruction of quantum microwave states as well as quantum correlation measurements are performed using a heterodyne receiver setup. This heterodyne detection setup is similar to the setups described in Refs. [24,35,36,51]. The signal is downconverted to 11 MHz and digitized by an Acqiris card with a sampling frequency of 400 MHz. The digitized data is transmitted to a computer and downconverted to a dc signal. The resulting signal is filtered using a digital finite-impulse-response (FIR) filter with a full bandwidth of 400 kHz. Subsequently, the quadrature moments $\langle I_1^n Q_1^m I_2^k Q_2^l \rangle$, $n, m, k, l \in \mathbb{N}_0$ are determined and averaged. In each measurement, the data is averaged over 210 cycles, where each cycle corresponds to 5.76×10^6 averages. The squeezing angles are stabilized using a phase-locked loop, where in each measurement cycle, the squeezing angle γ_i^{exp} is extracted from the quadrature moments corresponding to the ith JPA, where $i \in \{1, 2\}$. Following this approach, the difference $\delta\gamma_i = \gamma_i^{\text{exp}} - \gamma_i^{\text{target}}$ from the desired target angle γ_i^{target} is calculated and the respective phase of the JPA pump source is corrected by $2\delta\gamma_i$. The JPA pump sources are daisy chained with a reference frequency of 1 GHz to the LO source. The LO, the DTG, the VNA, and the AFG, as well as the Acqiris card are synchronized with a 10 MHz rubidium frequency clock (Stanford Research Systems, FS725). In our experiment, we assume that all reconstructed states are Gaussian and can be described by signal moments up to the second order. This assumption of Gaussianity is verified by calculating the cumulants κ_{mn} [52]. Since it is theoretically expected that $\kappa_{mn} = 0$ for $m + n > 2$ for Gaussian states, we conclude that the Gaussian approximation of our quantum states is well justified if the experimentally reconstructed cumulants of third and fourth order are much smaller than the first- and second-order cumulants.

2. Quantum key distribution with Gaussian states

In order to investigate the relation between the LII flow and QKD, we consider that Alice and Bob share an ideal TMS state with the squeezing factor r, described by the covariance matrix

$$V_{\text{AB}} = \frac{1}{4}\begin{pmatrix} \cosh 2r\, \mathbb{1}_2 & \sinh 2r\, \hat{\sigma}_z \\ \sinh 2r\, \hat{\sigma}_z & \cosh 2r\, \mathbb{1}_2 \end{pmatrix}, \tag{A1}$$

where $\mathbb{1}_2$ denotes the 2×2 identity matrix and $\hat{\sigma}_z$ is the Pauli z matrix. For the entangling cloner attack, the eavesdropper

prepares a second TMS state [48]

$$V_{\mathrm{E_1E_2}} = \frac{1}{4}\begin{pmatrix} W\mathbb{1}_2 & \sqrt{W^2-1}\,\hat{\sigma}_z \\ \sqrt{W^2-1}\,\hat{\sigma}_z & W\mathbb{1}_2 \end{pmatrix}. \tag{A2}$$

As a result, the full covariance matrix

$$V_{\mathrm{ABE_1E_2}} = V_{\mathrm{AB}} \oplus V_{\mathrm{E_1E_2}} \tag{A3}$$

describes a pure state. The eavesdropper then couples the mode E_1 to B by an asymmetric beam splitter operation

$$C = \begin{pmatrix} \sqrt{1-\beta}\,\mathbb{1}_2 & \sqrt{\beta}\,\mathbb{1}_2 \\ -\sqrt{\beta}\,\mathbb{1}_2 & \sqrt{1-\beta}\,\mathbb{1}_2 \end{pmatrix}. \tag{A4}$$

The resulting covariance matrix is given by

$$V'_{\mathrm{ABE_1E_2}} = (\mathbb{1}_2 \oplus C \oplus \mathbb{1}_2) V_{\mathrm{ABE_1E_2}} (\mathbb{1}_2 \oplus C \oplus \mathbb{1}_2)^\dagger, \tag{A5}$$

which can be analytically expressed as

$$V'_{\mathrm{ABE_1E_2}} = \frac{1}{4}\begin{pmatrix} V'_{11} & V'_{12} & V'_{13} & \mathbb{0}_2 \\ V'^{\mathrm{T}}_{12} & V'_{22} & V'_{23} & V'_{24} \\ V'^{\mathrm{T}}_{13} & V'^{\mathrm{T}}_{23} & V'_{33} & V'_{34} \\ \mathbb{0}_2 & V'^{\mathrm{T}}_{24} & V'^{\mathrm{T}}_{34} & V'_{44} \end{pmatrix}, \tag{A6}$$

where

$$\begin{aligned} V'_{11} &= \cosh 2r \mathbb{1}_2, \\ V'_{12} &= \sqrt{1-\beta}\,\sinh 2r\,\hat{\sigma}_z, \\ V'_{13} &= -\sqrt{\beta}\,\sinh 2r\,\hat{\sigma}_z, \\ V'_{22} &= (1-\beta)\cosh 2r \mathbb{1}_2 + \beta W \mathbb{1}_2, \\ V'_{23} &= \sqrt{\beta(1-\beta)}\,(W - \cosh 2r)\mathbb{1}_2, \\ V'_{24} &= \sqrt{\beta}\,\sqrt{W^2-1}\,\hat{\sigma}_z, \\ V'_{33} &= \beta\,\cosh 2r \mathbb{1}_2 + (1-\beta) W \mathbb{1}_2, \\ V'_{34} &= \sqrt{1-\beta}\,\sqrt{W^2-1}\,\hat{\sigma}_z, \\ V'_{44} &= W\mathbb{1}_2. \end{aligned} \tag{A7}$$

Since the matrix $V'_{22}/4$ corresponds to the local noisy TMS state in system B, we demand

$$\frac{1}{4}(\cosh 2r + 2n)\mathbb{1}_2 = \frac{1}{4}[(1-\beta)\cosh 2r\,\mathbb{1}_2 + \beta W \mathbb{1}_2]. \tag{A8}$$

In the limit $\beta \ll 1$, we find the relation $\beta W = 2n$. Since we perform a homodyne detection on B in the next step, it is practical to define the number of noise photons, added to the measured quadrature, as $n_q = n/2$. For the final state of the eavesdropper, we have

$$V'_{\mathrm{E}} = \frac{1}{4}\begin{pmatrix} V'_{33} & V'_{34} \\ V'^{\mathrm{T}}_{34} & V'_{44} \end{pmatrix}. \tag{A9}$$

We consider reverse reconciliation and hence perform a measurement of B [46]. After a homodyne measurement of the q quadrature, the conditioned covariance matrix for E reads

$$V'_{\mathrm{E|B}} = V'_{\mathrm{E}} - \frac{1}{4\sqrt{\det V'_{22}}} V'_{\mathrm{C}} \Pi_q V'^{\mathrm{T}}_{\mathrm{C}}, \tag{A10}$$

where $V_{\mathrm{C}} = (V'_{23}, V'_{24})^{\mathrm{T}}$ and Π_q denotes the phase-space projector on the q quadrature. The corresponding Holevo quantity χ_E is then obtained as

$$\chi_{\mathrm{E}} = S_{\mathrm{E}} - S_{\mathrm{E|B}}, \tag{A11}$$

where S_{E} ($S_{\mathrm{E|B}}$) denotes the von Neumann entropy, corresponding to V'_{E} ($V'_{\mathrm{E|B}}$) [48,49]. For a two-mode Gaussian state, described by a covariance matrix V, the von Neumann entropy is given by

$$S = f(\nu_+) + f(\nu_-), \tag{A12}$$

where ν_+ and ν_- are the symplectic eigenvalues of V [53]. For a codebook of input states with variance σ^2, the Shannon mutual information is obtained to be [48]

$$\begin{aligned} I_{\mathrm{s}}(\mathrm{A:B}) &= \frac{1}{2}\log_2(1+\mathrm{SNR}) \\ &= \frac{1}{2}\log_2\left(1 + \frac{4(1-\beta)\sigma^2}{(1-\beta)e^{-2r} + 4n_q}\right) \\ &\simeq \frac{1}{2}\log_2\left(1 + \frac{\sigma^2}{n_q}\right), \end{aligned} \tag{A13}$$

where the last expression is valid in the limit $r \gg 1$ and $\beta \ll 1$. For the calculation of the signal-to-noise ratio (SNR) in the detected quadrature, we have considered the protocol described in Ref. [19], implying a noise of $e^{-2r}/4 + n_q$ per quadrature and $\sigma^2 = \sinh(2r)/2$. To obtain Fig. 3, we have fixed $\beta = 10^{-4}$.

3. Fitting the experimental data

In this section, we provide details about the model used to fit the experimental data. By taking finite coupling and amplifier noise into account, the final covariance matrix can be expressed as

$$V_{\mathrm{AB}} = \frac{1 + 2n_{\mathrm{j}}(G)}{4}\begin{pmatrix} \boldsymbol{\alpha} & \boldsymbol{\gamma} \\ \boldsymbol{\gamma}^{\mathrm{T}} & \boldsymbol{\beta} \end{pmatrix}, \tag{A14}$$

where

$$\boldsymbol{\alpha} = \cosh 2r\,\mathbb{1}_2, \tag{A15}$$

$$\boldsymbol{\beta} = [(1-\beta)\cosh 2r + \beta(1+2\bar{n})]\mathbb{1}_2, \tag{A16}$$

$$\boldsymbol{\gamma} = \sqrt{1-\beta}\,\sinh 2r\,\hat{\sigma}_z. \tag{A17}$$

Furthermore, $n_{\mathrm{j}}(G)$ represents the noise added by the JPAs, which depends on the degenerate gain G. In addition, $\bar{n}$ is the number of noise photons at the input of the coupled port of the directional coupler. The environmental noise $\bar{n}$ is related to n via $n = \beta\bar{n}$ under the assumption that $\bar{n} \gg 1$. The realistic squeezing factor r can be extracted from the reconstructed squeezed (antisqueezed) variance v_{s} (v_{a}) via $e^{4r} = v_{\mathrm{a}}/v_{\mathrm{s}}$. The degenerate gain can then be expressed as $G = e^{2r}$. Furthermore, we model the gain-dependent JPA noise by a power-law dependence $n_{\mathrm{j}}(G) = \chi_1(G-1)^{\chi_2}$, where we treat χ_1 and χ_2 as the only fit parameters. For the fit, we use $\boldsymbol{\chi} \equiv (\chi_1, \chi_2)^{\mathrm{T}}$ and define a corresponding weighted least-square cost

function

$$T(\boldsymbol{\chi}) = \sum_{S,n} (w_1 |D_{\mathrm{A}}(S,n,\boldsymbol{\chi}) - \tilde{D}_A(S,n)|^2 + w_2 |D_{\mathrm{B}}(S,n,\boldsymbol{\chi}) - \tilde{D}_B(S,n)|^2 + w_3 |E_{\mathrm{F}}(S,n,\boldsymbol{\chi}) - \tilde{E}_{\mathrm{F}}(S,n)|^2), \tag{A18}$$

where the sum is evaluated over all experimentally chosen squeezing levels S and noise photon numbers n. The quantities w_i are the weights, accounting for the respective contribution. The quantities $\tilde{D}_A(S,n)$, $\tilde{D}_B(S,n)$, and $\tilde{E}_{\mathrm{F}}(S,n)$ are the experimentally determined data points for A discord, B discord, and EOF, respectively, corresponding to S and n. The functions $D_{\mathrm{A}}(S,n,\boldsymbol{\chi})$, $D_{\mathrm{B}}(S,n,\boldsymbol{\chi})$, and $E_{\mathrm{F}}(S,n,\boldsymbol{\chi})$ are obtained by inserting Eq. (A14) into the theoretical expressions for QD and EOF. The fit parameters $\chi_1 = 0.05$ and $\chi_2 = 0.56$ are then given by

$$\begin{pmatrix} \chi_1 \\ \chi_2 \end{pmatrix} = \underset{\boldsymbol{\chi}}{\mathrm{argmin}} T(\boldsymbol{\chi}), \tag{A19}$$

where we start with the initial conditions $\boldsymbol{\chi} = (0,1)^{\mathrm{T}}$. To balance the contributions of QD and EOF in the cost function, we choose the weights $w_1 = w_2 = 1/2$ and $w_3 = 1$ for the fit. To extract the noise photon numbers corresponding to the sudden death of entanglement as well as the experimental crossover points between QD and EOF, we do not make use of the fit curves. Instead, we determine these values directly from the experimental data using cubic Hermite spline interpolation as we expect this method to be more accurate than the fit. We use cubic Hermite spline interpolation instead of conventional cubic splines to increase the precision by avoiding overshoots.

[1] S. L. Braunstein and P. van Loock, Quantum information with continuous variables, Rev. Mod. Phys. **77**, 513 (2005).

[2] Z. Chen, K. J. Satzinger, J. Atalaya, A. N. Korotkov, A. Dunsworth, D. Sank *et al.*, Exponential suppression of bit or phase errors with cyclic error correction, Nature (London) **595**, 383 (2021).

[3] A. Eddins, M. Motta, T. P. Gujarati, S. Bravyi, A. Mezzacapo, C. Hadfield, and S. Sheldon, Doubling the size of quantum simulators by entanglement forging, PRX Quantum **3**, 010309 (2022).

[4] F. Arute, K. Arya, R. Babbush, D. Bacon, J. C. Bardin, R. Barends *et al.*, Quantum supremacy using a programmable superconducting processor, Nature (London) **574**, 505 (2019).

[5] X. Wang, T. Hiroshima, A. Tomita, and M. Hayashi, Quantum information with Gaussian states, Phys. Rep. **448**, 1 (2007).

[6] S. L. Braunstein and H. J. Kimble, Dense coding for continuous variables, Phys. Rev. A **61**, 042302 (2000).

[7] K. G. Fedorov, M. Renger, S. Pogorzalek, R. Di Candia, Q. Chen, Y. Nojiri *et al.*, Experimental quantum teleportation of propagating microwaves, Sci. Adv. **7**, eabk0891 (2021).

[8] A. Furusawa, J. L. Sørensen, S. L. Braunstein, C. A. Fuchs, H. J. Kimble, and E. S. Polzik, Unconditional quantum teleportation, Science **282**, 706 (1998).

[9] H. Ollivier and W. H. Zurek, Quantum Discord: A Measure of the Quantumness of Correlations, Phys. Rev. Lett. **88**, 017901 (2001).

[10] A. Datta, A. Shaji, and C. M. Caves, Quantum Discord and the Power of One Qubit, Phys. Rev. Lett. **100**, 050502 (2008).

[11] B. P. Lanyon, M. Barbieri, M. P. Almeida, and A. G. White, Experimental Quantum Computing without Entanglement, Phys. Rev. Lett. **101**, 200501 (2008).

[12] D. Girolami, A. M. Souza, V. Giovannetti, T. Tufarelli, J. G. Filgueiras, R. S. Sarthour, D. O. Soares-Pinto, I. S. Oliveira, and G. Adesso, Quantum Discord Determines the Interferometric Power of Quantum States, Phys. Rev. Lett. **112**, 210401 (2014).

[13] C. Weedbrook, S. Pirandola, J. Thompson, V. Vedral, and M. Gu, How discord underlies the noise resilience of quantum illumination, New J. Phys. **18**, 043027 (2016).

[14] C. Weedbrook, S. Pirandola, R. García-Patrón, N. J. Cerf, T. C. Ralph, J. H. Shapiro, and S. Lloyd, Gaussian quantum information, Rev. Mod. Phys. **84**, 621 (2012).

[15] F. F. Fanchini, L. K. Castelano, M. F. Cornelio, and M. C. de Oliveira, Locally inaccessible information as a fundamental ingredient to quantum information, New J. Phys. **14**, 013027 (2012).

[16] D. Girolami, A. Touil, B. Yan, S. Deffner, and W. H. Zurek, Redundantly Amplified Information Suppresses Quantum Correlations in Many-Body Systems, Phys. Rev. Lett. **129**, 010401 (2022).

[17] W. H. Zurek, Quantum darwinism, Nat. Phys. **5**, 181 (2009).

[18] A. Touil, B. Yan, D. Girolami, S. Deffner, and W. H. Zurek, Eavesdropping on the Decohering Environment: Quantum Darwinism, Amplification, and the Origin of Objective Classical Reality, Phys. Rev. Lett. **128**, 010401 (2022).

[19] N. J. Cerf, M. Lévy, and G. Van Assche, Quantum distribution of Gaussian keys using squeezed states, Phys. Rev. A **63**, 052311 (2001).

[20] T. Yu and J. H. Eberly, Sudden death of entanglement, Science **323**, 598 (2009).

[21] M. Sanz, K. G. Fedorov, F. Deppe, and E. Solano, Challenges in open-air microwave quantum communication and sensing, in *Proceedings of the 2018 IEEE Conference on Antenna Measurements & Applications (CAMA)* (IEEE, New York, 2018), pp. 1–4.

[22] T. Werlang, S. Souza, F. F. Fanchini, and C. J. Villas Boas, Robustness of quantum discord to sudden death, Phys. Rev. A **80**, 024103 (2009).

[23] C. H. Bennett, D. P. DiVincenzo, P. W. Shor, J. A. Smolin, B. M. Terhal, and W. K. Wootters, Remote State Preparation, Phys. Rev. Lett. **87**, 077902 (2001).

[24] S. Pogorzalek, K. G. Fedorov, M. Xu, A. Parra-Rodriguez, M. Sanz, M. Fischer *et al.*, Secure quantum remote state preparation of squeezed microwave states, Nat. Commun. **10**, 2604 (2019).

[25] B. Dakić, Y. O. Lipp, X. Ma, M. Ringbauer, S. Kropatschek, S. Barz *et al.*, Quantum discord as resource for remote state preparation, Nat. Phys. **8**, 666 (2012).

[26] S. Lloyd, Enhanced sensitivity of photodetection via quantum illumination, Science **321**, 1463 (2008).
[27] S. Tserkis and T. C. Ralph, Quantifying entanglement in two-mode Gaussian states, Phys. Rev. A **96**, 062338 (2017).
[28] P. Giorda and M. G. A. Paris, Gaussian Quantum Discord, Phys. Rev. Lett. **105**, 020503 (2010).
[29] G. Adesso and A. Datta, Quantum versus Classical Correlations in Gaussian States, Phys. Rev. Lett. **105**, 030501 (2010).
[30] F. F. Fanchini, M. F. Cornelio, M. C. de Oliveira, and A. O. Caldeira, Conservation law for distributed entanglement of formation and quantum discord, Phys. Rev. A **84**, 012313 (2011).
[31] S. Tserkis, S. Onoe, and T. C. Ralph, Quantifying entanglement of formation for two-mode Gaussian states: Analytical expressions for upper and lower bounds and numerical estimation of its exact value, Phys. Rev. A **99**, 052337 (2019).
[32] L. Henderson and V. Vedral, Classical, quantum and total correlations, J. Phys. A: Math. Gen. **34**, 6899 (2001).
[33] T. Yamamoto, K. Inomata, M. Watanabe, K. Matsuba, T. Miyazaki, W. D. Oliver, Y. Nakamura, and J. S. Tsai, Flux-driven Josephson parametric amplifier, Appl. Phys. Lett. **93**, 042510 (2008).
[34] E. P. Menzel, R. Di Candia, F. Deppe, P. Eder, L. Zhong, M. Ihmig, M. Haeberlein, A. Baust, E. Hoffmann, D. Ballester, K. Inomata, T. Yamamoto, Y. Nakamura, E. Solano, A. Marx, and R. Gross, Path Entanglement of Continuous-Variable Quantum Microwaves, Phys. Rev. Lett. **109**, 250502 (2012).
[35] K. G. Fedorov, L. Zhong, S. Pogorzalek, P. Eder, M. Fischer, J. Goetz, E. Xie, F. Wulschner, K. Inomata, T. Yamamoto, Y. Nakamura, R. Di Candia, U. Las Heras, M. Sanz, E. Solano, E. P. Menzel, F. Deppe, A. Marx, and R. Gross, Displacement of Propagating Squeezed Microwave States, Phys. Rev. Lett. **117**, 020502 (2016).
[36] K. G. Fedorov, S. Pogorzalek, U. Las Heras, M. Sanz, P. Yard, P. Eder *et al.*, Finite-time quantum entanglement in propagating squeezed microwaves, Sci. Rep. **8**, 6416 (2018).
[37] E. Flurin, N. Roch, F. Mallet, M. H. Devoret, and B. Huard, Generating Entangled Microwave Radiation Over Two Transmission Lines, Phys. Rev. Lett. **109**, 183901 (2012).
[38] C. Eichler, D. Bozyigit, C. Lang, M. Baur, L. Steffen, J. M. Fink, S. Filipp, and A. Wallraff, Observation of Two-Mode Squeezing in the Microwave Frequency Domain, Phys. Rev. Lett. **107**, 113601 (2011).
[39] M. Mariantoni, E. P. Menzel, F. Deppe, M. Á. Araque Caballero, A. Baust, T. Niemczyk, E. Hoffmann, E. Solano, A. Marx, and R. Gross, Planck Spectroscopy and Quantum Noise of Microwave Beam Splitters, Phys. Rev. Lett. **105**, 133601 (2010).
[40] S. Tserkis, J. Thompson, A. P. Lund, T. C. Ralph, P. K. Lam, M. Gu, and S. M. Assad, Maximum entanglement of formation for a two-mode Gaussian state over passive operations, Phys. Rev. A **102**, 052418 (2020).
[41] S. Luo, Quantum discord for two-qubit systems, Phys. Rev. A **77**, 042303 (2008).
[42] P. Marian, I. Ghiu, and T. A. Marian, Decay of Gaussian correlations in local thermal reservoirs, Phys. Scr. **90**, 074041 (2015).
[43] M. Renger, S. Pogorzalek, Q. Chen, Y. Nojiri, K. Inomata, Y. Nakamura *et al.*, Beyond the standard quantum limit for parametric amplification of broadband signals, npj Quantum Inf. **7**, 160 (2021).
[44] V. C. Usenko, L. Ruppert, and R. Filip, Entanglement-based continuous-variable quantum key distribution with multimode states and detectors, Phys. Rev. A **90**, 062326 (2014).
[45] O. Ahonen, M. Möttönen, and J. L. O'Brien, Entanglement-enhanced quantum key distribution, Phys. Rev. A **78**, 032314 (2008).
[46] F. Grosshans, N. J. Cerf, J. Wenger, R. Tualle-Brouri, and P. Grangier, Virtual entanglement and reconciliation protocols for quantum cryptography with continuous variables, Quantum Inf. Comput. **3**, 535 (2003).
[47] F. Fesquet, F. Kronowetter, M. Renger, Q. Chen, K. Honasoge, O. Gargiulo *et al.*, Perspectives of microwave quantum key distribution in open-air, arXiv:2203.05530 (2022).
[48] F. Laudenbach, C. Pacher, C. F. Fung, A. Poppe, M. Peev, B. Schrenk, M. Hentschel, P. Walther, and H. Hübel, Continuous-variable quantum key distribution with Gaussian modulation–the theory of practical implementations, Adv. Quantum Technol. **1**, 1800011 (2018).
[49] A. S. Holevo, Bounds for the quantity of information transmitted by a quantum communication channel, Probl. Inf. Transm. **9**, 177 (1973).
[50] L. Zhong, E. P. Menzel, R. Di Candia, P. Eder, M. Ihmig, A. Baust *et al.*, Squeezing with a flux-driven Josephson parametric amplifier, New J. Phys. **15**, 125013 (2013).
[51] S. Pogorzalek, K. G. Fedorov, L. Zhong, J. Goetz, F. Wulschner, M. Fischer *et al.*, Hysteretic Flux Response and Nondegenerate Gain of Flux-Driven Josephson Parametric Amplifiers, Phys. Rev. Appl. **8**, 024012 (2017).
[52] S. H. Xiang, W. Wen, Y. J. Zhao, and K. H. Song, Evaluation of the non-Gaussianity of two-mode entangled states over a bosonic memory channel via cumulant theory and quadrature detection, Phys. Rev. A **97**, 042303 (2018).
[53] A. Serafini, F. Illuminati, and S. De Siena, Symplectic invariants, entropic measures and correlations of Gaussian states, J. Phys. B: At. Mol. Opt. Phys. **37**, L21 (2004).